DOI: 10.1002/ppap.200500065

Summary: In this paper, some of our modeling efforts for processing plasmas are presented. We make use of fluid models or particle-in-cell–Monte Carlo (PIC-MC) simulations for the plasma behavior, depending on the application. Fluid models are most suitable to describe the detailed plasma chemistry, like the formation and growth of nanoparticles in so-called dusty plasmas, and for dielectric barrier discharges (DBDs) at atmospheric pressure. PIC-MC simulations are the best choice to describe magnetron discharges, operating at low pressure, and for dealing with the plasma dynamics in single- and dual-frequency rf discharges. Finally, we also apply molecular dynamics (MD) simulations for plasma-surface interaction, more specifically for the plasma deposition of diamond-like carbon (DLC) films.

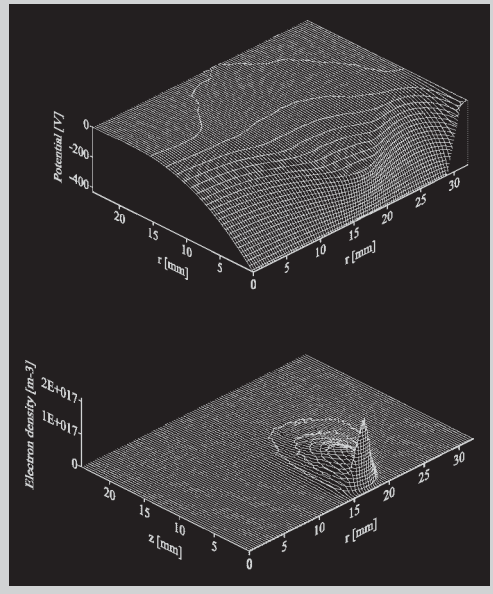

Calculated potential distribution and electron density profile in the magnetron discharge.

Computer Simulations for Processing Plasmas

Annemie Bogaerts, Kathleen De Bleecker, Violeta Georgieva, Ivan Kolev, Myriam Madani, Erik Neyts*

PLASMANT Research group, Department of Chemistry, University of Antwerp, Universiteitsplein 1, B-2610 Wilrijk-Antwerp, Belgium
Fax: (+32) 3 820.23.76; E-mail: annemie.bogaerts@ua.ac.be

Received: August 31, 2005; Revised: October 28, 2005; Accepted: November 4, 2005; DOI: 10.1002/ppap.200500065

Keywords: computer modeling; fluid model; molecular dynamics; particle-in-cell Monte Carlo

Introduction

Gas discharges find increasing importance in materials technology, e.g., for plasma etching, thin film deposition, surface modification, etc. To improve these applications, a good insight into the plasma behavior is desirable. In our research group PLASMANT, we try to obtain this by numerical modeling.

In the literature, there exist different modeling approaches for processing plasmas. In ***analytical models***,[1] analytical formulas describe the dependency of certain plasma quantities from macroscopic parameters (e.g., voltage, current). This method can quickly predict the plasma behavior, but it is only an approximation, valid for a limited range of conditions.

A ***fluid model***[2] is based on the continuity equations of particle density, momentum, and energy, usually coupled to Poisson's equation to calculate a self-consistent electric field distribution. It is in principle also quite simple and fast, but it assumes that the plasma species are more or less in equilibrium with the electric field, i.e., the energy gain from the electric field is more or less balanced by the energy loss due to collisions. This is not always true, e.g., at low gas pressure, and for the fast electrons in regions characterized by a strong electric field.

By solving the ***Boltzmann transport equation***,[3] the non-equilibrium behavior of the plasma species is fully accounted for. However, this approach can become mathematically very complicated.

Monte Carlo (MC) simulations,[4] on the other hand, are mathematically simple, and they also account correctly for the non-equilibrium behavior of the plasma species. They describe the trajectories of individual particles by Newton's laws, and treat the collisions by random numbers. In order to reach statistically valid results, a large number of individual particles need to be simulated. Hence, MC simulations can be very time-consuming, especially for slow-moving particles. Moreover, a MC model on its own is not ''self-consistent'', because it requires a certain electric field distribution as input value.

This problem is overcome by the *particle-in-cell–Monte Carlo (PIC-MC)* method,[5] which couples MC simulations for the behavior of ions and electrons, to the Poisson equation for a self-consistent electric field distribution. This method is particularly interesting for discharges at very low pressure, where the plasma species can have high energies and are not in equilibrium with the electric field, or when the detailed plasma dynamics needs to be simulated. It is, however, not so suitable to describe the plasma chemistry in great detail, because it becomes too time-consuming for a large number of different plasma species.

Finally, ***hybrid models***[6] are a combination of different models for the different species (e.g., MC models for fast plasma species, which are not in equilibrium with the electric field, and fluid models for slow species, which can be considered in thermal equilibrium).

It is clear that every modeling approach has its own advantages and disadvantages, and will be most suitable for a specific kind of problem. In our group, we mainly make use of fluid models and PIC-MC simulations, although we have developed comprehensive hybrid models as well, describing the behavior of various plasma species.[6,7] Moreover, we also try to simulate the plasma-wall interactions, for instance, the processes taking place in thin film deposition. For this purpose, we use ***molecular dynamics (MD) simulations***,[8] which treat the processes by Newton's laws, using the interaction potentials between all species. In the following, we will give a few examples of our modeling efforts for processing plasmas. Although the examples given here are adopted from our own research group, the principles of using a particular model for a certain application are quite general, and are also valid for other modeling activities in the literature.

Fluid Modeling

In a fluid model, a large number of different plasma species can be treated. Hence, this model approach is particularly suitable for describing the detailed plasma chemistry. For every species, a continuity equation (i.e., a balance equation, taking into account all different production and loss mechanisms) and a transport equation (which is a modified version of the momentum conservation equation; see above) is constructed. Transport is based on diffusion for the neutral species (molecules, radicals) and on diffusion and migration under influence of the electric field for the charged particles (ions, electrons). For the conservation of energy, an energy balance equation (describing energy gain from the electric field and energy losses due to collisions) is included for the electrons. For the other plasma species, no energy balance equation is incorporated because they are assumed to be in thermal equilibrium. Finally, these equations are coupled to Poisson's equation for a self-consistent calculation of the electric field distribution. This yields a system of non-linear coupled differential equations, which are solved numerically with the Scharfetter-Gummel exponential scheme.[9]

Fluid Model for Describing Nanoparticle Formation in So-called Dusty Plasmas

Nanoparticle (or dust) formation has been observed in many processing plasmas. For some applications, this is considered to be harmful because the nanoparticles can contaminate the substrate, but on the other hand, nanoparticles in plasmas can also lead to very interesting applications. For instance, amorphous silicon thin film deposition in solar cell applications seems to benefit from the presence of nanoparticles because the latter can be incorporated in the growing films, resulting in the production of a new material, i.e., polymorphous silicon, with superior electric properties, hence being a good candidate for use in high-efficiency solar cells.[10]

We have developed a fluid model for a capacitively coupled (cc) radiofrequency (rf) discharge in silane, in order to investigate the mechanisms of formation and growth of the nanoparticles, to describe their behavior in the plasma, and ultimately to predict under which conditions the nanoparticles can be incorporated in the deposited film. The fluid model describes the first stage of nanoparticle formation and growth, i.e., the nucleation phase.[11,12] Starting from silane (SiH_4), larger molecules are formed. 68 different species are considered in the model, including molecules, radicals, positive and negative ions, and electrons (see Table 1). For every Si_nH_{2n+2} molecule, the corresponding Si_nH_{2n+1} radical has to be considered, since H abstraction is an important reaction in silane plasmas. The silylenes Si_nH_{2n}, which are a reactive form of the silenes, and are characterized by a single bond between the two silicon atoms with two non-bonding electrons, are also included, since their corresponding anions play a role in the cluster growth. While the positive ions are limited to SiH_3^+, $Si_2H_4^+$, and H_2^+, the negative ions are extended up to species containing 12 Si atoms, because they determine the reaction pathway of nanoparticle growth.[13] The reason is that they are confined in the plasma by the positive plasma potential, so that they have a longer lifetime, and can play an important role in chemical reactions. A distinction is made

Table 1. Overview of the different species incorporated in the fluid model for a SiH_4 cc rf discharge for describing nanoparticle formation.

Molecules	Ions	Radicals	Electrons
SiH_4, $SiH_4^{(2-4)}$, $SiH_4^{(1-3)}$	SiH_3^+, $Si_2H_4^+$, H_2^+	SiH_3, SiH_2	e^-
H_2	SiH_3^-, SiH_2^-	H	
Si_nH_{2n+2} ($n=2$–12)	$Si_nH_{2n+1}^-$ ($n=2$–12)	Si_nH_{2n+1} ($n=2$–12)	
	$Si_nH_{2n}^-$ ($n=2$–12)	Si_nH_{2n} ($n=2$–12)	

between the silyl anions ($Si_nH_{2n+1}^-$) and the silylene anions ($Si_nH_{2n}^-$), because they correspond to the different sets of radicals.

Figure 1 shows the calculated density profiles of the various molecules: (a) radicals, (b) positive ions, (c) electrons, and (d) negative ions for a cc rf discharge, at a pressure of 40 Pa and a power of 5 W. It is clear that the anion SiH_3^- is the most important primary precursor of the particle formation. Over 90% of the nanoparticle formation proceeds through the silyl anion ($Si_nH_{2n+1}^-$) pathway, starting from SiH_3^-, and only about 10% goes through the silylene anion ($Si_nH_{2n}^-$) pathway, starting from SiH_2^-. More details about this model (e.g., importance of various chemical reaction mechanisms, etc) can be found in ref.[11,12]

The cluster growth in our fluid model stops at Si_nH_m species with 12 Si atoms, because it is not possible to describe the detailed plasma chemistry for an unlimited

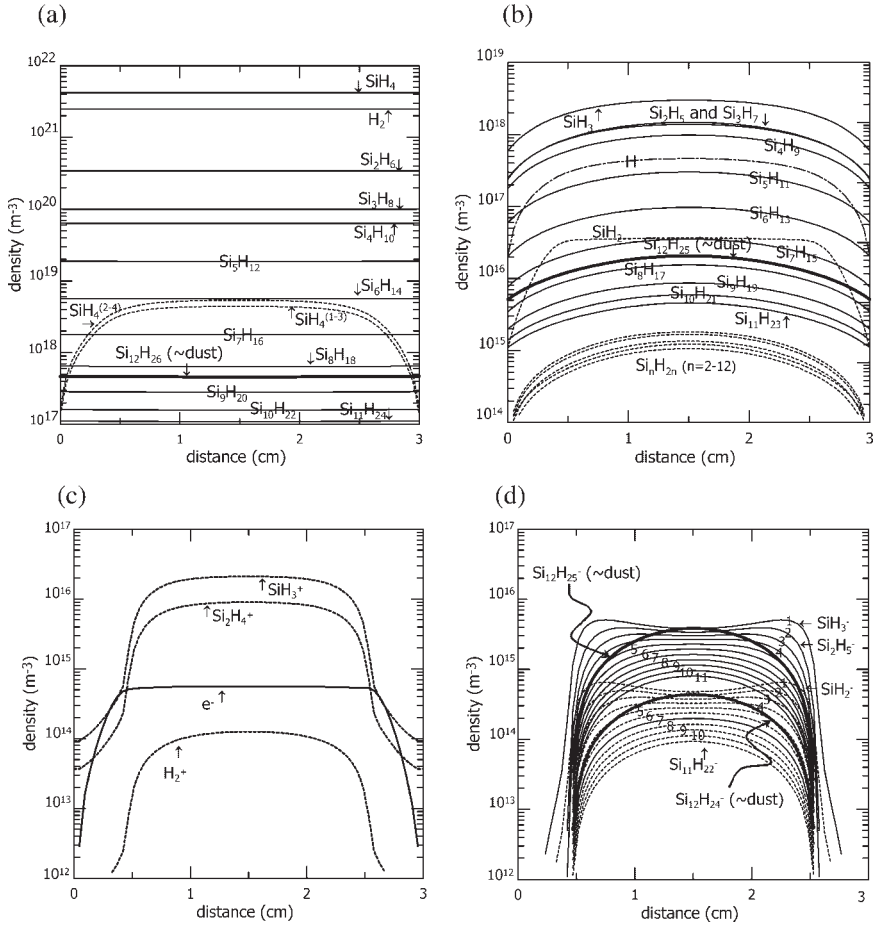

Figure 1. Calculated time-averaged density profiles of the Si_nH_{2n+2} molecules and the vibrationally excited SiH_4 molecules (a), the silyl radicals (Si_nH_{2n+1}) and the silylenes (Si_nH_{2n}) (b), the positive ions and electrons (c), and the various negative ions (d) for a cc rf discharge in SiH_4, at a pressure of 40 Pa and a power of 5 W. The numbers labeling the curves in d correspond to the number of Si atoms in the anions. Reproduced from ref.[11] with permission of the American Physical Society.

number of plasma species. The further growth is assumed to take place by coagulation, and will be described with an aerosol dynamics model,[14,15] which will be coupled self-consistently with our fluid model in the near future.

Beside the formation and growth of the nanoparticles, their charge and their dynamic behavior, as a result of different forces, are also is described in the model.[16] The average charge is calculated based on the orbital-motion-limited (OML) theory.[17] Briefly, the floating potential (V_{fl}) of the nanoparticles is obtained by equating the positive and negative currents (from positive ions and from negative ions or electrons, respectively) to the nanoparticle, and the corresponding charge is given by: $Q = 4\pi\varepsilon_0 r_d V_{fl}$, where r_d is the nanoparticle radius. Because the electron current is always higher than the positive ion current, due to their smaller mass, the nanoparticles will nearly always be negatively charged. In the near future, we also want to include random fluctuations to this average charge, due to the individual collection of electrons and ions. In this way, the charge of the smallest nanoparticles ($\approx$ few nanometers) can fluctuate from slightly negative till slightly positive, so that these nanoparticles might be able to escape the positive plasma potential and reach the substrate, where they can become incorporated in the depositing layer, or contaminate the substrate. For this reason, a good knowledge about the charge of the nanoparticles is very important.

Finally, the transport of the nanoparticles is not only dictated by diffusion and migration anymore but also influenced by other forces, such as gravity, ion drag, neutral drag, and thermophoretic force (as a result of a temperature difference). This leads to a modified flux equation, as is explained in detail in ref.[16,18] In practice, the gravitation force can be neglected for the sub-micrometer particles under consideration in our study, and the neutral drag force acts only as a damping force on the velocity of the nanoparticles, in absence of a considerable gas flow. Figure 2 and 3 illustrate the effect of the remaining forces (i.e., electrostatic force, ion drag, and thermophoretic force, in the case of a temperature difference between both electrodes) on nanoparticles with two different sizes (i.e., 30 and 100 nm in diameter, respectively). In the absence of a temperature difference, it is found that for particles of diameter 30 nm or less, the electrostatic force is predominant, resulting in a density profile with its maximum in the center of the discharge [see Figure 2(a)]. Larger nanoparticles will experience the ion drag force and are pushed toward the reactor boundaries, until the force is balanced by the electrostatic force. This leads to the trapping of the nanoparticles in some well-defined region near the plasma-sheath boundary [see Figure 3(a)].[16] When a temperature difference, as small as 20 K, is applied between both electrodes, e.g., when the grounded electrode is heated to a temperature of 320 K and the powered electrode is kept at 300 K, the particles immediately experience the extra thermophoretic force, and the profile shifts toward the cooler electrode, as is clearly seen in Figure 2(b) and 3(b) for the particles of 30 and 100 nm, respectively.[18] Hence, it will be the dynamic competition between the different forces that causes a nanoparticle of a certain size to levitate in some well-defined region in the plasma.

Fluid Model for an Atmospheric Pressure Dielectric Barrier Discharge (DBD)

We have also recently developed a fluid model for a dielectric barrier discharge (DBD) in N_2 at 1 atm, typically used for deposition and activation of layers.[19] Indeed, at

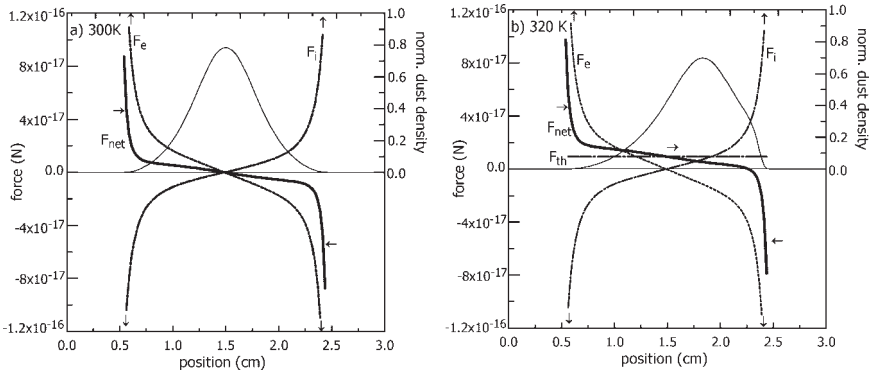

Figure 2. Calculated electric force (F_e), ion drag force (F_i), thermophoretic force (F_{th}), and net force (F_{net}) acting on nanoparticles of 30 nm, (a) when there is no temperature difference between the electrodes, and (b) when there is a temperature difference of 20 K [i.e., grounded electrode (at 0 cm) is heated to 320 K, and powered electrode (at 3 cm) is kept at 300 K]. The forces are only presented in the bulk region of the discharge, i.e., between 0.5 and 2.5 cm, where they attain the same order of magnitude. The direction of the net force, represented by a thicker solid line, is indicated by left and right arrows. The resulting density profile is also shown by a thin solid line, right axis. Reproduced from ref.[18] with permission of the American Physical Society.

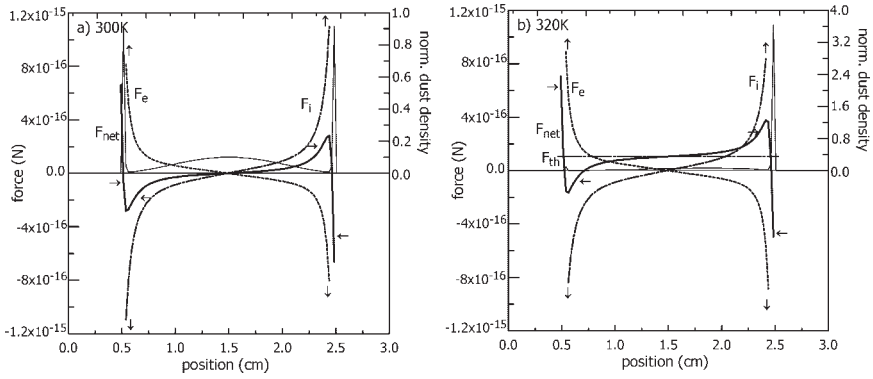

Figure 3. Calculated electric force (F_e), ion drag force (F_i), thermophoretic force (F_{th}), and net force (F_{net}) acting on nanoparticles of 100 nm, (a) when there is no temperature difference between the electrodes, and (b) when there is a temperature difference of 20 K. The forces are only presented in the bulk region of the discharge, i.e., between 0.5 and 2.5 cm, where they attain the same order of magnitude. The direction of the net force, represented by a thicker solid line, is indicated by left and right arrows. The resulting density profile is also shown by a thin solid line, right axis. Reproduced from ref.[18] with permission of the American Physical Society.

such high pressure, the plasma species undergo many collisions, so that they are more or less in equilibrium with the electric field. Hence, a fluid model is the most straightforward approach. The species taken into account in this model are N_2 molecules, N atoms, N_2 molecules in four excited states (i.e., two metastable and two radiative levels), N^+, N_2^+, N_3^+, and N_4^+ ions.

Beside the usual equations of a fluid model, some additional equations have to be solved in the fluid model for the DBD. Indeed, the DBD consists of two parallel electrodes, of which at least one is covered with an insulating material (dielectric), and this needs to be taken into account by using the appropriate boundary conditions for the potential. Moreover, secondary electron emission and electron desorption from the dielectric, when the polarity of the electric field is switched, have to be taken into account as well, by adding two extra terms for the electron flux at the boundary. Hence, this results also in a modified boundary condition for the electron density, compared to a fluid model for a discharge between two conducting electrodes. More details can be found in ref.[19]

It is well known that an atmospheric pressure DBD can yield a uniform or a filamentary discharge, and the uniform DBD can be either in glow mode or in Townsend mode, depending on the frequency, discharge voltage, width of the discharge gap, and the kind of dielectric and its thickness.[20] In the glow mode, the electron and ion densities in the bulk of the discharge are nearly equal to each other, like in a low-pressure glow discharge. In the Townsend mode, on the other hand, the electron density rises from the instantaneous cathode to the instantaneous anode, and the ion density exceeds the electron density by several orders of magnitude, so that there is no charge neutrality in the plasma.[20] Hence, from the density profiles calculated with our model, we can derive which kind of discharge mode is expected for certain discharge conditions.

Figure 4 shows the calculated density profiles of electrons and the various ions in a DBD under two different conditions: (a) a DBD with ceramic dielectrics, at a frequency of 2 kHz, a voltage of 13 kV (peak-to-peak), and a discharge gap of 1 mm; and (b) a DBD with PEN [poly(ethylene naphthalene)] foils as dielectrics, at a frequency of 12.8 kHz, a voltage of 13 kV (peak-to-peak), and a discharge gap of 1.2 mm. The calculated time profiles of current and voltage for both DBD conditions were carefully checked with experimental data, and very good agreement was reached,[19] which proves that our model works properly for both conditions. It is clear that the kind of dielectric (and the frequency) has a pronounced effect on the operation regime of the DBD. In the first case, the DBD appears to be in Townsend mode, because the electron density is several orders of magnitude lower than the ion densities. In the second case, however, a glow-like structure was obtained, with equal densities for ions and electrons.

PIC-MC Modeling

Fluid modeling is very useful for describing the detailed plasma chemistry, but it is not so accurate for low gas pressure, and it does not provide information related to the detailed plasma dynamic behavior, as for example for the electron and ion energy distribution functions (IEDFs). For these purposes, PIC-MC simulations are the more logical choice, because they treat the individual plasma particles and accurately account for the energy gain from the electric field and energy losses through collisions.[21]

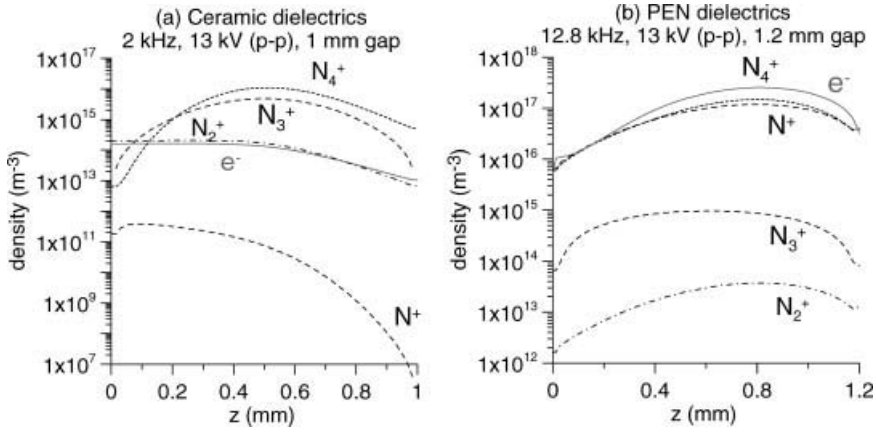

Figure 4. Calculated density profiles of the electrons and the various ions, throughout the discharge, at $\omega t = \pi/2$, for a DBD in N_2, under two different operating conditions. The instantaneous anode is located at $z = 0$ mm, whereas the instantaneous cathode is at $z = 1$ or 1.2 mm, respectively.

In a PIC-MC model, charged particles (ions and electrons) are replaced by superparticles, with a weight (i.e., number of real particles per superparticle) in the order of 10^7 to 10^9 (depending on the ion and electron densities). The movement of the superparticles under the influence of the electric field (and magnetic field, in the case of magnetron discharges) is simulated with Newton's laws, during successive time-steps. After each time-step, the charge density is calculated from the particles' coordinates and assigned to the computational grid nodes, on which the Poisson equation is solved. This yields a new electric field on each grid node, which is linearly interpolated to each particle position. Then, the particles are moved again during the next time-step. The collisions (i.e., occurrence of a collision during each time-step, kind of collision and new energy and direction after collision) are treated with random numbers, in the Monte Carlo part of the model. By following a large number of superparticles, the detailed behavior of the plasma species (ions and electrons) can be statistically simulated.

PIC-MC Model for a Magnetron Discharge in Argon

Since magnetron discharges, used for sputter-deposition of thin films, operate at low pressure (order of several mTorr), a PIC-MC model is the natural choice. We have developed a PIC-MC model for a dc planar magnetron discharge, as is shown in Figure 5. The magnet is placed behind the target, and the magnetic field strengths are indicated with the arrows. The maximum magnetic field strength (cf. largest arrows in the figure) is found in front of the target, at about 1.8 cm from the cylinder axis. Because the applied magnetic field and the magnetron discharge reactor are both axi-symmetric, the whole system can be considered as cylindrically symmetrical, so that the PIC-MC model can be reduced to a cylindrical (r,z) coordinate space.

Beside the electrons and Ar^+ ions, our PIC-MC model also simulates the behavior of fast Ar atoms, sputtered (Cu) atoms, and the corresponding Cu^+ ions. Further, the entire model for the magnetron discharge includes modules for gas heating, and for diffusive transport of sputtered Cu atoms (after thermalization) and of Ar metastable atoms (which play an important role in Penning ionization of the sputtered Cu atoms). Finally, a simple model for the external circuit is included, to calculate the current and voltage in a fully self-consistent way. More information about this PIC-MC model for magnetron discharges can be found in ref.[22]

Figure 6 illustrates the calculated potential distribution (a), electron density (b), and sputtered Cu atom density

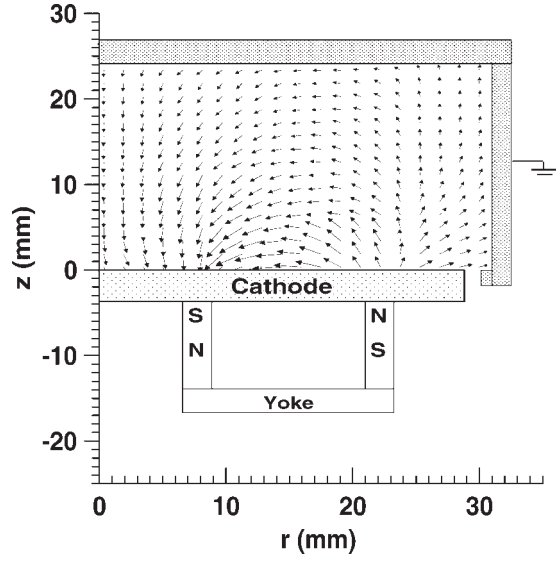

Figure 5. Schematic diagram of the magnetron discharge under study, indicating the dimensions, the magnets, as well as the magnetic field lines. The length of the arrows indicates the magnitude of the magnetic field strength. The maximum magnetic field is 1 200 G.

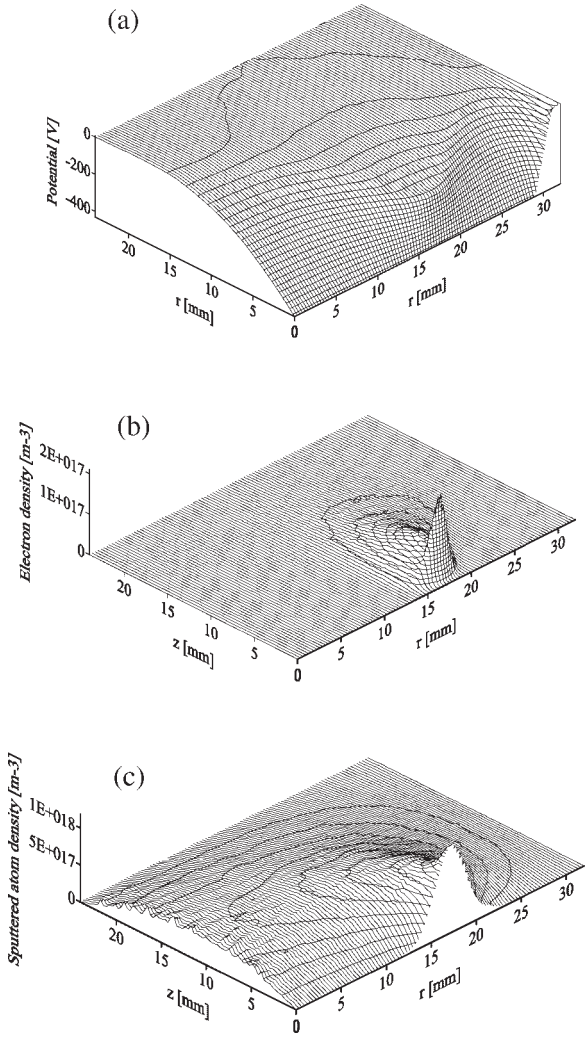

Figure 6. Calculated potential distribution (a), electron density profile (b), and sputtered Cu atom density profile (c) in the magnetron discharge shown in Figure 5, at an argon gas pressure of 5 mTorr, a maximum magnetic field of 1 200 G, and an external voltage of 550 V, corresponding to a discharge voltage of about 400 V.

profile (c) for a magnetron discharge operating at 5 mTorr with 550 V external voltage (resulting in a discharge voltage of 400 V) and maximum magnetic field of 1 200 G. It is clear from this figure that the cathode dark space is the shortest, and hence the electric field is the strongest, at about 1.8 cm from the cylinder axis, i.e., where the magnetic field strength is at its maximum. Also the electron density reaches a maximum in this region because (i) most electrons are created here by electron impact ionization because they gain most energy from the electric field, and (ii) the electrons are trapped in the magnetic field lines. The sputtered Cu atoms are characterized by a broader distribution [see Figure 6(c)]. The peak near the target is due to the fast Cu atoms, immediately after sputtering, whereas the broad distribution is due to diffusion of thermalized Cu

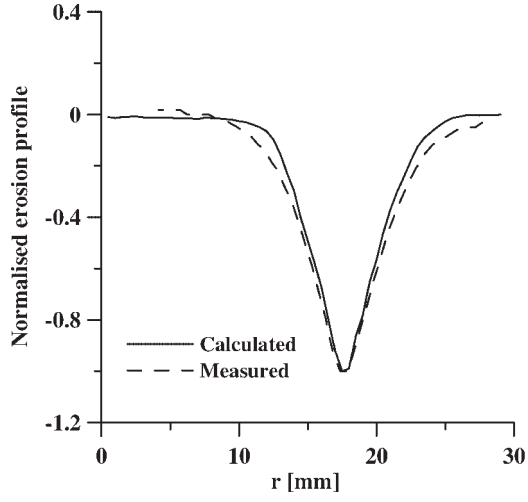

Figure 7. Calculated (solid line) and measured (dashed line) normalized erosion profiles at the target, as a result of sputtering, for the same conditions as in Figure 6, after 4 h of sputtering.

atoms. However, due to the low pressure and the relatively small dimensions of the magnetron discharge under study, there is a non-negligible fraction of Cu atoms with energies of a few eV, which reach the substrate.

To check the correctness of the model the calculated erosion profile, as a result of sputtering, is compared to the experimentally measured one[23] under approximately the same operating conditions, after 4 h of sputtering, and the agreement was very satisfactory, as is illustrated in Figure 7. Both maxima coincide perfectly and the shape of the crater is almost identical.

PIC-MC Model for a Single- and Dual-Frequency cc rf Discharge in $CF_4/Ar/N_2$

Plasma etching by cc rf discharges is well recognized for its anisotropy, which is a critical process parameter in integrated circuit manufacturing. To study the detailed dynamic behavior of ions and electrons in such kind of plasma, and to calculate the EEDFs and (especially) IEDFs, which are important quantities for etching applications, we have developed a PIC-MC model for a cc rf reactor, in a mixture of $CF_4/Ar/N_2$.[24,25] This is a typical gas mixture used for plasma etching of silicon and SiO_2 in the semiconductor industry. The model considers the following species: electrons, Ar^+, CF_3^+, N_2^+, F^-, and CF_3^- ions. 41 different electron-neutral collisions, two electron-ion recombination reactions, four positive-negative ion recombination reactions, and about 130 ion-neutral chemical reactions are incorporated in the model (see ref.[24,25] for more details).

Recently, there is increased interest in dual-frequency cc rf reactors (i.e., applying two frequencies instead of one) because they allow independent control of ion bombardment energy and ion flux toward the substrate (e.g., ref.[26]).

In addition, a dual-frequency setup provides a wider ion bombardment energy in comparison with a single-frequency scheme. Therefore, we have studied in detail the behavior of dual-frequency cc rf discharges in a mixture $Ar/CF_4/N_2$, and comparison is made with single-frequency reactors.[25,27,28] Figure 8 illustrates calculated IEDFs at the powered electrode, for Ar^+, CF_3^+, and N_2^+ ions, averaged over one rf-cycle in the single-frequency (13.56 MHz) cc rf reactor (a), and averaged over two low-frequency (LF) cycles in the dual-frequency (2 + 27 MHz) reactor (b). The reason that averaging is performed over two LF cycles is because one LF cycle does not contain an integer number of high-frequency (HF) cycles.[25]

It is indeed clear that the IEDFs in the single-frequency reactor are quite narrow, with one outstanding peak (for CF_3^+), and possibly secondary peaks at lower energy, because of energy losses through collisions (as is the case for Ar^+ and N_2^+). The IEDFs in the dual-frequency reactor, on the other hand, are broad and bimodal, and the two outstanding peaks in the profiles correspond to the averaged minimum and maximum sheath potential drop.[25,27] Further, the IEDF width depends on the ion mass, i.e., a lower mass (e.g., for N_2^+) yields a somewhat broader IEDF. More information about this study of single- and dual-frequency cc rf reactors can be found in ref.[25,27]

We have also studied the influence of HF and LF voltages on several plasma quantities, to investigate in detail under which conditions independent control of ion flux and energy is possible.[28] Figure 9 shows the effect of HF or LF voltage on the total ion current density at the electrodes [Figure 9(a) and (b), respectively] and on the average ion bombardment energy of the three different positive ions (Ar^+, N_2^+, and CF_3^+) at the electrode [Figure 9(c) and (d)], for a 60 + 2 MHz dual-frequency reactor. Calculation results for a single-frequency (60 MHz) reactor are also illustrated in Figure 9(a) and (c), with gray lines. It appears that the ion current density is somewhat lower, and the average ion energy is somewhat higher in the dual-frequency reactor, i.e., when a second, LF voltage is present. Further, it is clearly seen that both HF and LF voltages influence the ion bombardment energy to the same extent, and that the average ion energy is merely determined by the sum of HF and LF voltages. On the other hand, only the HF voltage seems to affect the ion current density, as is clear from Figure 9(a) and (b). Hence, independent control of ion energy and flux is possible, by applying a second (LF) voltage. We performed an extensive study for a wide range of different combinations of HFs and LFs, and it was concluded that independent control of ion flux and bombardment energy was only obtained for HFs of 60 MHz and above.[28]

MD Simulations

Finally, modeling the plasma-wall interactions is also very important for most applications of processing plasmas. This can be performed by MD simulations, which describe the behavior of the plasma species arriving at the substrate, by means of interatomic interaction potentials. We present here results of an MD model for the plasma deposition of amorphous hydrogenated carbon (a:C–H) layers, by means of the Brenner potential for hydrocarbons.[29] The model is applied to typical experimental conditions for the deposition of a:C–H layers in an expanding thermal Ar/C_2H_2 plasma (ETP).[30] The input in the model, i.e., the fluxes and energies of the species bombarding the substrate, are taken from experiment. Typical results of the model include the DLC film structure and composition, more specifically, the bonding network, the film density, the H content, and the coordination number of C atoms,[31,32] as well as detailed information about the sticking mechanisms of the various species playing a role in the film growth.

It is demonstrated experimentally that C_3H and C_3 are the most important species contributing to the film growth in

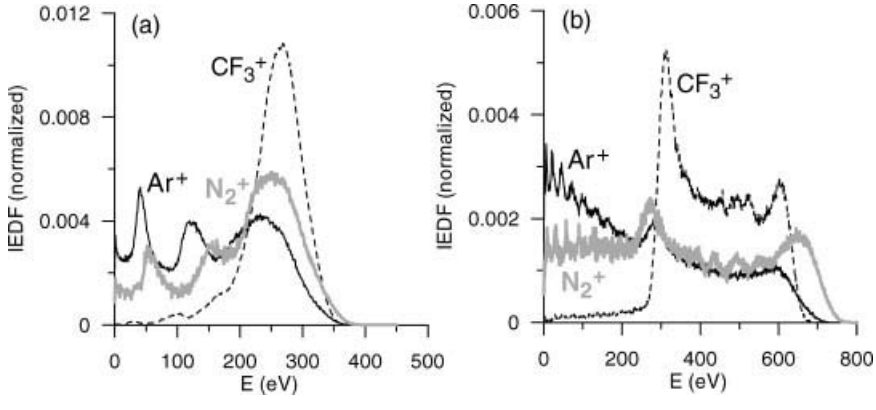

Figure 8. Calculated time-averaged ion energy distribution functions (IEDF) at the powered electrode, for Ar^+, CF_3^+, and N_2^+ ions, at a pressure of 30 mTorr and a voltage amplitude of 700 V, in (a) a single-frequency (13.56 MHz) cc rf reactor and (b) a dual-frequency (2 + 27 MHz) reactor.

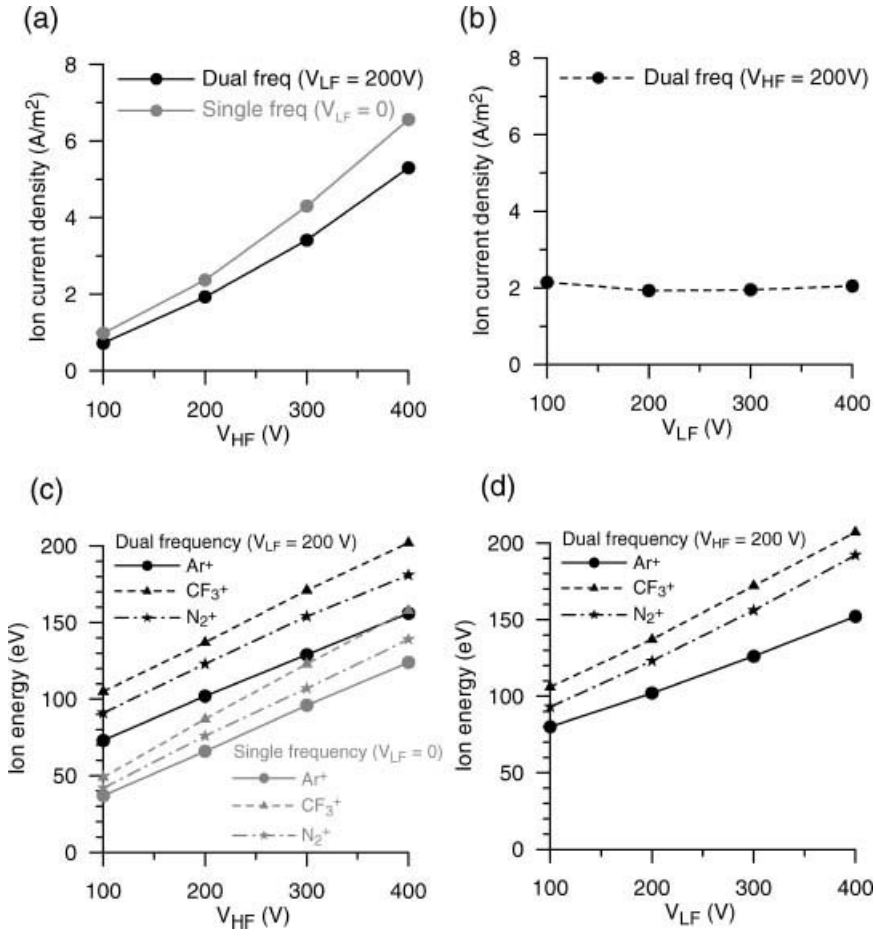

Figure 9. Calculated total ion current density at the electrodes, as a function of HF voltage (a) and LF voltage (b), and calculated average ion bombardment energy of the three different positive ions (Ar^+, N_2^+, and CF_3^+) at the electrodes, as a function of HF voltage (c) and LF voltage (d), for a 60 + 2 MHz dual-frequency reactor. The effect of HF voltage in a single-frequency (60 MHz) reactor is also presented in (a) and (c), with gray lines.

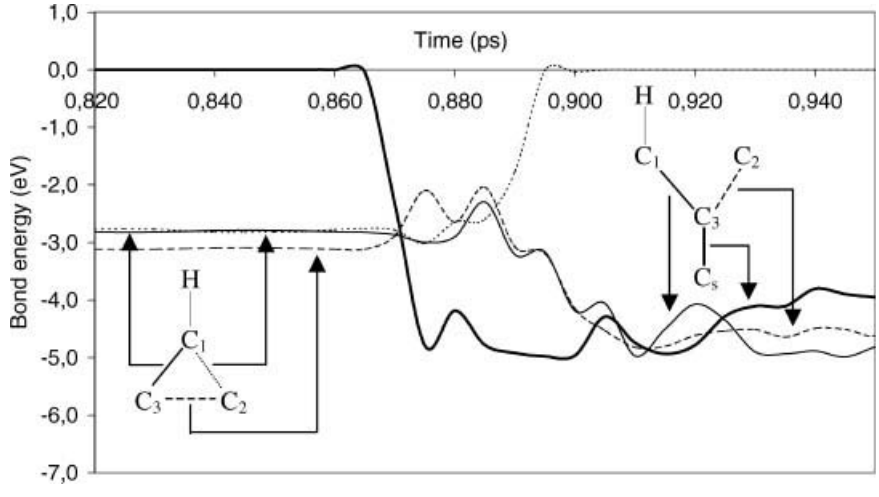

Figure 10. Calculated energy of the different bonds in c-C_3H upon sticking on an amorphous hydrogenated carbon (a:C–H) surface, showing the detailed sticking mechanism.

ETPs at high fluxes of acetylene.[33] Because it is not clear whether the cyclic or linear isomers of these species play a role, we have investigated and compared their reaction mechanisms by MD simulations.[34] As an example, Figure 10 shows the change in bond energy upon sticking of a cyclic C_3H radical on an a:C–H surface. The different curves denote different C–C bonds in the radical, whereas the thicker curve represents the bond between a C atom of the radical and a C atom of the surface (denoted as C_s). Before sticking, the C_1–C_3 bond and C_1–C_2 bond in the radical are slightly weaker than the C_3–C_2 bond. Note that all three bonds are clearly weaker than a normal single C–C bond (which has a typical energy of 3.6 eV) because of the severe ring strain in the radical. At ca. 0.86 ps, the radical reacts at the surface, with formation of a bond between the C_3 atom of the radical and the C_s atom of the surface. Simultaneously, the C_1–C_2 bond breaks (bond energy goes to zero), and the other bonds first become slightly weaker, but then become stronger, with a bond energy of about 4.5 eV, which is similar to the bond energy of the created bond between the radical and the surface. Hence, this means that three similar bonds are formed between C_3 and the three surrounding C atoms (including the surface). Based on the bond energy, it can be concluded that these three bonds lie in between a single C–C bond and a double bond (with bond energy of 3.6 and 6.4 eV, respectively).

Conclusion

In this paper, we have presented a few examples of our modeling work for gas discharge plasmas used for materials science applications. Depending on the kind of problem, either fluid modeling or PIC-MC simulations are employed for the plasma behavior. Fluid models are particularly suitable for describing detailed plasma chemistry, but they are not so good for low gas pressure, where the plasma species can gain more energy from the electric field than they lose by collisions. In this case, PIC-MC simulations are a better choice. Moreover, they allow to give a more detailed description of the plasma dynamics (e.g., ion and electron energy distribution functions, collision processes, etc.). For the description of plasma-wall interactions, more specifically the deposition of DLC layers, MD simulations are the most logical choice.

The examples show what kind of information can be expected from numerical modeling. In general, a better insight into the plasma behavior is acquired, which will be helpful for making progress in the application fields.

Acknowledgements: K. De Bleecker and E. Neyts acknowledge financial support from *IWT*. M. Madani is supported from the *Flemish Institute for Technological Research* (VITO). The research is also sponsored by the IAP-V program.

[1] Y. T. Lee, M. A. Lieberman, A. J. Lichtenberg, F. Bose, H. Baltes, R. Patrick, *J. Vac. Sci. Technol.* **1997**, *15*, 113.
[2] J. D. P. Passchier, W. J. Goedheer, *J. Appl. Phys.* **1993**, *73*, 1073.
[3] D. Loffhagen, F. Sigeneger, R. Winkler, *J. Phys. D: Appl. Phys.* **2002**, *35*, 1768.
[4] Z. Donko, K. Rozsa, R. C. Tobin, *J. Phys. D: Appl. Phys.* **1996**, *29*, 105.
[5] M. Surendra, D. B. Graves, *IEEE Trans. Plasma Sci.* **1991**, *19*, 144.
[6] A. Bogaerts, R. Gijbels, W. J. Goedheer, *J. Appl. Phys.* **1995**, *78*, 2233.
[7] A. Bogaerts, *Plasma Sources Sci. Technol.* **1999**, *8*, 210.
[8] M. A. Karolewski, *Surf. Int. Anal.* **1999**, *27*, 114.
[9] D. L. Scharfetter, H. K. Gummel, *IEEE Trans. Electron. Devices* **1969**, *16*, 64.
[10] P. Roca i Cabarrocas, A. Fontcuberta i Morral, Y. Poissant, *Thin Solid Films* **2002**, *403–404*, 39.
[11] K. De Bleecker, A. Bogaerts, R. Gijbels, W. Goedheer, *Phys. Rev. E* **2004**, *69*, 056409.
[12] K. De Bleecker, A. Bogaerts, W. Goedheer, R. Gijbels, *IEEE Trans. Plasma Sci.* **2004**, *32*, 691.
[13] U. V. Bhandarkar, M. T. Swihart, S. L. Girshick, U. R. Kortshagen, *J. Phys. D: Appl. Phys.* **2000**, *33*, 2731.
[14] U. Kortshagen, U. Bhandarkar, *Phys. Rev. E* **1999**, *60*, 887.
[15] J. D. Landgrebe, S. E. Pratsinis, *J. Colloid Interface Sci.* **1990**, *139*, 63.
[16] K. De Bleecker, A. Bogaerts, W. Goedheer, *Phys. Rev. E* **2004**, *70*, 056407.
[17] J. E. Allen, B. M. Annaratone, U. De Angelis, *J. Plasma Phys.* **2000**, *63*, 299.
[18] K. De Bleecker, A. Bogaerts, W. Goedheer, *Phys. Rev. E* **2005**, *71*, 066405.
[19] M. Madani, A. Bogaerts, D. Vangeneugden, *J. Appl. Phys.* (submitted).
[20] Yu. B. Golubovskii, V. A. Maiorov, J. Behnke, J. F. Behnke, *J. Phys. D: Appl. Phys.* **2003**, *36*, 39.
[21] C. K. Birdsall, A. B. Langdon, "*Plasma Physics via Computer Simulations*", McGraw-Hill, New York 1985.
[22] I. Kolev, A. Bogaerts, R. Gijbels, *Phys. Rev. E* **2005**, *72*, 056402.
[23] G. Buyle, private communication.
[24] V. Georgieva, A. Bogaerts, R. Gijbels, *J. Appl. Phys.* **2003**, *93*, 2369.
[25] V. Georgieva, A. Bogaerts, R. Gijbels, *J. Appl. Phys.* **2003**, *94*, 3748.
[26] K. Maeshige, G. Washio, T. Yagisawa, T. Makabe, *J. Appl. Phys.* **2002**, *91*, 9494.
[27] V. Georgieva, A. Bogaerts, R. Gijbels, *Phys. Rev. E* **2004**, *69*, 026406.
[28] V. Georgieva, A. Bogaerts, *J. Appl. Phys.* **2005**, *98*, 023308.
[29] D. W. Brenner, *Phys. Rev. B* **1990**, *42*, 9458.
[30] J. Benedikt, K. G. Y. Letourneur, M. Wisse, D. C. Schram, M. C. M. van de Sanden, *Diamond Relat. Matec.* **2002**, *11*, 989.
[31] E. Neyts, A. Bogaerts, R. Gijbels, J. Benedikt, M. C. M. van de Sanden, *Diamond Relat. Matec.* **2004**, *13*, 1873.
[32] E. Neyts, A. Bogaerts, R. Gijbels, J. Benedikt, M. C. M. van de Sanden, *Nucl. Instr. Methods B* **2005**, *228*, 315.
[33] J. Benedikt, S. Agarwal, D. Eijkman, W. Vandamme, M. Creatore, M. C. M. van de Sanden, *J. Vac. Sci. Technol. A* **2005**, *23*, 1400.
[34] E. Neyts, A. Bogaerts, M. C. M. van de Sanden, *J. Appl. Phys.* **2006** (in press).

